Spatiotemporal-MIMO Channel Estimator and Beamformer for 5G

Vidhya Sridhar, *IEEE Student Member*, Thibaud Gabillard, *IEEE Student Member*, and Athanassios Manikas, *IEEE Senior Member*

***Abstract*—With requirements of spiralling data rates and limited spectrum availability, there is an increased interest in mm-wave beamformer-based communications for 5G. For upcoming cellular networks, the critical point is to exploit the increased number of employable antennas at both Tx and Rx to (i) combat increased path loss, (ii) tackle higher interference due to higher user density and (iii) handle multipath effects in frequency selective channels. Towards this, a multi-beam spatiotemporal superresolution beamforming framework is proposed in this paper as a promising candidate to design beampatterns that mitigate/suppress co-channel interference and deliver massive gain in the desired directions. Initially, channel and signal models suitable for the mm-wave MIMO system are presented using the manifold vectors of both Tx and Rx antenna arrays. Based on these models, a novel subspace-based channel estimator is employed which estimates delays, directions, velocities and fading coefficients of the desired signal paths. This information is then exploited by the proposed spatiotemporal beamformer to provide massive array gain that combats path loss without increasing the number of antenna array elements and to be tolerant to the near-far problem in a high interference environment. The performance of the proposed channel estimator and beamformer is examined using computer simulation studies.**

***Index Terms*—MIMO, frequency selective channel, mm-wave, spatiotemporal beamformer, channel estimation.**

NOTATION

A, a	Scalar
$\underline{A}$, $\underline{a}$	Column vector
$\mathbb{A}$	Matrix
$(\cdot)^T$, $(\cdot)^H$	Transpose, Hermitian transpose
$(\cdot)^*$, $(\cdot)^\#$	Complex conjugate, Pseudo-inverse
$\lceil a \rceil$	Smallest integer greater than or equal to a
$\lfloor a \rfloor$	Largest integer smaller than or equal to a
$\mathcal{E}\{\cdot\}$	Expectation operator
$\mathrm{Tr}\{\mathbb{A}\}$	Trace of $\mathbb{A}$
$\mathrm{diag}\{\underline{A}\}$	Diagonal matrix whose diagonal elements are the elements of $\underline{A}$
$\exp(\underline{A})$	Element by element exponential of vector $\underline{A}$
$\mathrm{vec}\,(\mathbb{A})$	Column-wise vectorisation of $\mathbb{A}$
$\mathrm{col}_m\,(\mathbb{A})$	m-th column of $\mathbb{A}$
$\mathrm{eig}_m(\mathbb{A})$	m-th eigenvalue of $\mathbb{A}$
$\mathrm{eig}_{\min}(\mathbb{A})$	Minimum eigenvalue of $\mathbb{A}$
$\odot$, $\otimes$	Hadamard product, Kronecker product
$\mathbb{I}_N$	$N \times N$ Identity matrix
$\underline{1}_N$, $\underline{0}_N$	Column vector of N ones, zeros
$\mathcal{R}$, $\mathcal{C}$	Set of real numbers, set of complex numbers

I. INTRODUCTION

One of the major concerns that 5G wireless communications attempts to address is the ability to support the ever-growing demand of data rates and predicted exponential increase in traffic volumes. Towards this end, the unutilised millimetre wave (mm-wave) frequency band is seen as a promising candidate to augment the already saturated lower frequency bands for wireless communications. However, a major limitation at these frequencies is the increased propagation losses [1]. In addition, the mm-wave channel is known to be frequency selective [2], [3], [4], while foliage losses and rain attentuation for the mm-wave are significant and can limit the coverage severely. Furthermore, attenuation factors due to obstacles in non-line-of-sight (NLOS) communications are much higher as compared to their counterparts in the 1-3 GHz communications band. Another critical problem would be the interference management arising from high user density in small cell deployments. In such environments, typical power control mechanisms will be much harder to operate. Some of these interfering users may be closer ("near") to the receiver than the desired user ("far"), transmitting with relatively higher power than that of the desired user which may be far away, resulting in extremely high interference levels. The performance of the subspace technique proposed in this paper is independent of the interference to signal power ratio, also known as near-far ratio (NFR), making it more suitable to handle the well known near-far problem *without* the need of power control. Lastly, at these frequencies, the size of the antenna elements shrinks. This enables designers to integrate many more antenna elements onto the user-end devices as compared to the conventional radio frequency communication bands.

Some research to demonstrate the practicability of mm-wave beamformer systems has been done in [5], [6] and particularly the mitigation of interference cancellation using beamspace multiple-input multiple-output (MIMO) has been discussed in [7]. Outdoor propagation measurements carried out in the 28 GHz band illustrate that simple beam combining in itself can improve gain, counteract pathloss and shadow fading [8]. For the special case of a weak line-of-sight (LOS) path, a diversity eigenbeamformer has been proposed [9] which utilises the eigendecomposition of the channel covariance matrix. In [10], a precoding scheme (i.e. Tx beamforming) has been proposed assuming a known channel and no multiple access interference (MAI). Furthermore, in [11], using a uniform linear array, a pilot-based direction of arrival (DOA) estimator for the paths of a single user (no MAI) has been proposed. However, the absence of MAI (or failure to isolate interference from noise) and ignoring other channel parameters renders the solutions of [10] and [11] incomplete. In a number of proposed beamformer solutions for mm-wave, the strategy

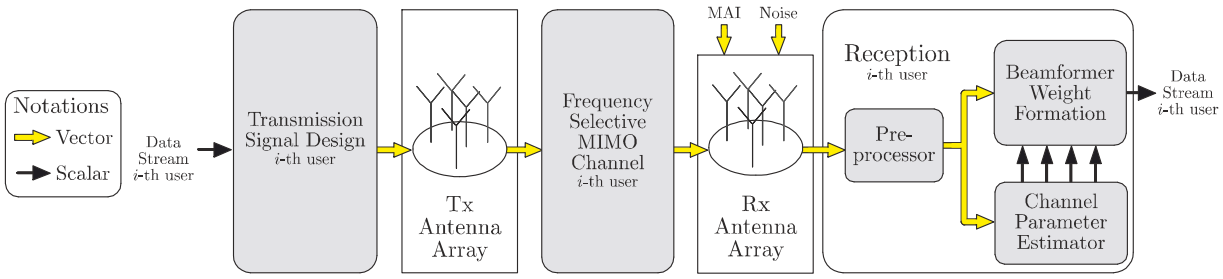

Fig. 1: Basic representation of the proposed system consisting of signal design, MIMO channel model and receiver for the i-th user. The Rx antenna array operates as a physical vector adder adding the received signals from the i-th user, its MAI and noise effects.

of hybrid beamforming, i.e. combining analog and digital beamforming, has been employed. This is with the objective of reducing design complexity and power burden arising from the numerous analogue front-end chains to support the increased number of antennas. In [12], a hybrid beamformer consisting of analogue subarrays and a digital beamformer has been proposed. However, it exploits the spatial dimension alone and employs an expensive iterative DOA estimation procedure requiring more iterations at a lower signal-to-noise ratio (SNR). A hybrid beamformer maximizing the receiver output SNR has been proposed in [13].

The majority of the proposed mm-wave beamformers use criteria such as maximizing SNR, signal-to-noise-plus-interference ratio (SNIR) or minimising the bit error rate (BER). However, these beamformers are built around a traditional "non-parametric" model while the proposed channel model in this paper belongs to the family of "parametric". Traditional MIMO channel models, although very popular, are "debatable" in the sense that they ignore the array geometry, which is one of the most important known parameter of interest of any antenna array system. In this case, the channel is modelled by the "channel state information" (CSI) matrix whose elements are the overall path gains from each Tx antenna to each Rx antenna (rather than from Tx array to Rx array), devouring in this way the array geometry. Consequently, the estimation of the CSI is complex and in many cases impractical for a large antenna array system. This is reflected by the fact that in a vast number of MIMO papers the CSI is assumed to be known. On the other hand, parametric models are based on wave propagation characteristics/properties from the Tx antenna array to the Rx antenna array and model the channel in terms of its parameters such as operational frequency, Tx array geometry, Rx array geometry, number of multipaths and their associated directions, relative path delays, Doppler frequency shifts and complex path fading coefficients. Thus, the clear advantage of the proposed parametric channel model is that powerful channel estimation is possible and practical which is not the case with the traditional (non-parametric) MIMO channel model.

The SpatioTemporal ARray (STAR) manifold beamformer proposed in this paper integrates space and time[1] in a single manifold vector, called the spatiotemporal manifold vector. This considerably empowers the receiver to provide narrow spatiotemporal multi-beams and combat the path loss by focusing the antenna array gain towards a specific path's directions of interest at the right time (delay). Figure 1 provides a basic representation of the proposed system. Unlike earlier systems, the proposed beamformer explicitly compensates MAI and estimates DOA, delay, radial velocity (Doppler frequency) and complex path gains of all paths of the desired user. Also, the channel estimation algorithm employed is blind, unlike systems with pilots such as in [14]. These form the main contributions of this paper. Note that this is different from the spatiotemporal approaches discussed in [15] and [16], where due to a non-parametric approach, that ignores the array geometry and DOAs, an original estimate of the interference subspace is assumed known. An iterative channel identification approach has been utilised leading to high complexity that increases with the number of interferers and number of antennas, making it unsuitable for the large antenna arrays of future 5G systems.

The remainder of the paper is organised as follows. In Section II, the spatiotemporal MIMO communications system, under consideration in this paper, is modelled in terms of the array manifold vectors of both Tx and Rx arrays for a frequency selective MIMO channel. In Section III, the design of the proposed spatiotemporal beamformer and its associated multi-parameter channel estimator is presented. In Section IV, computer simulation studies are employed to evaluate the performance of the proposed approach under various scenarios. Finally, in Section V the paper is concluded.

II. MIMO Communications System Model

Consider an M user MIMO system where the transmitter and receiver utilise antenna arrays consisting of $\overline{N}$ and N antenna elements respectively, with all users operating simultaneously on the same frequency band. For the i-th user, the MIMO system model is split into the transmitter, channel and receiver entities/blocks which are described and mathematically modelled below.

A. Transmitter Model

Each of the M co-channel users employs a unique PN-code of period $\mathcal{N}_c$ and a set of $\mathcal{N}_{sc}$ orthogonal subcarriers. With

[1]Please note that the concept of "space-time" here is not related/connected to space-time coding.

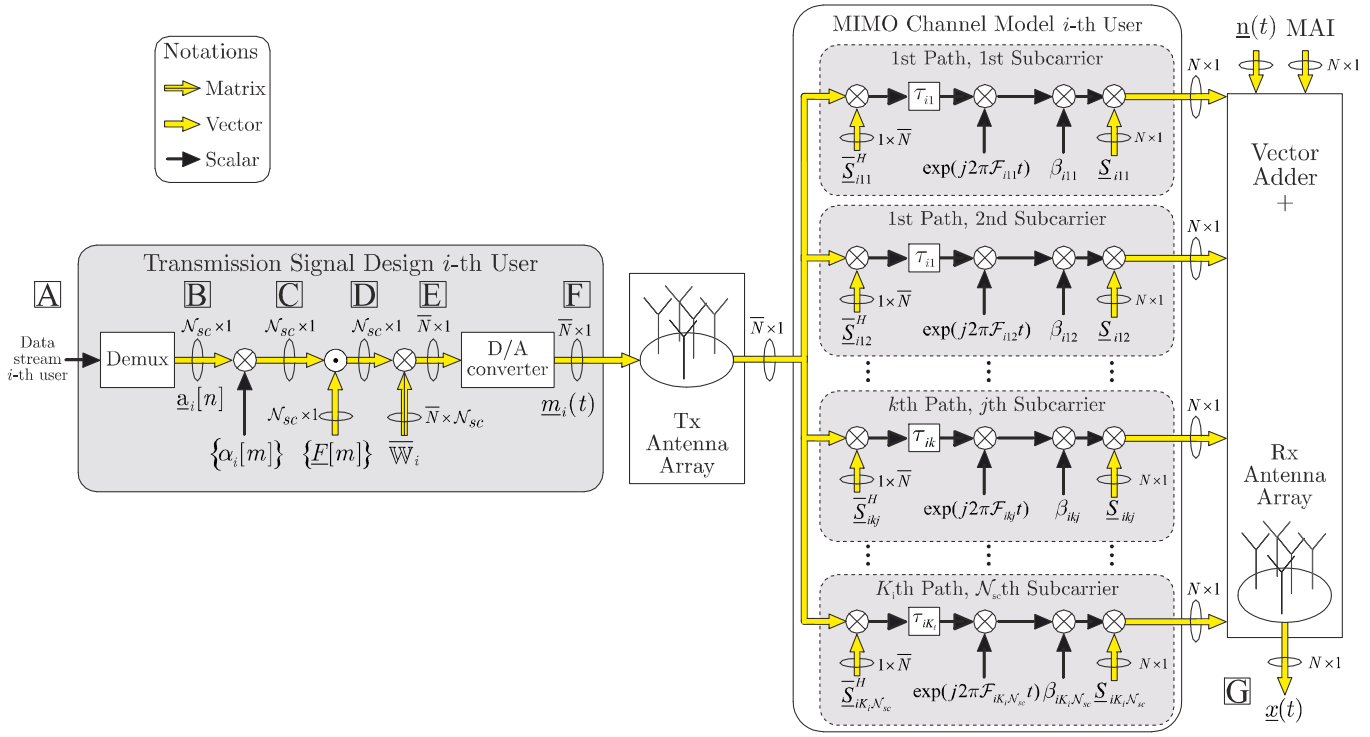

Fig. 2: Baseband representation of the transmitter and the MIMO channel for the i-th user of the proposed system. Each subcarrier per path is modelled in terms of the Tx and Rx array geometries, path delay, Doppler frequency, complex path fading coefficient, DOA and DOD.

reference to Fig 2, consider at point A the input data symbol stream of the i-th user. This stream is demultiplexed into $\mathcal{N}_{sc}$ streams represented by the vector sequence $\{\underline{a}_i[n]\}$,$\forall n$ (see point B). Each element of the transmitted symbol vector $\underline{a}_i[n] \in C^{\mathcal{N}_{sc}\times 1}$ is assumed to be of unity magnitude (without any loss of generality). Then, the data stream vector $\{\underline{a}_i[n]\}$, with a symbol period[2] T_{cs}, is spread by a PN-code sequence[3] of chip period T_c and sampling period T_s assigned to the i-th user. Let us define the vector $\underline{c}_i$ such that

$$\underline{c}_i = \underbrace{[\alpha_i[1], \alpha_i[2], \ldots, \alpha_i[\mathcal{N}_c]]^T}_{\text{one PN-code period}} \in \{+1, -1\}. \quad (1)$$

With $T_{cs} = \mathcal{N}_c T_c = \mathcal{N}_c\mathcal{N}_{sc}T_s$ at point C, for the $(\mathcal{N}_c\mathcal{N}_{sc}n + m)$-th interval, the transmitted vector at point C is given by $\underline{a}_i[n]\,\alpha_i\left[\left\lceil\frac{m}{\mathcal{N}_{sc}}\right\rceil\right]$, $\forall m \in \{1, 2, \ldots, \mathcal{N}_c\mathcal{N}_{sc}\}$. This is then modulated onto the set of $\mathcal{N}_{sc}$ subcarriers denoted by the vector $\underline{F}[m]$ given as

$$\underline{F}[m] = \exp\left(\mathrm{j}2\pi \begin{bmatrix} F_1 \\ \vdots \\ F_j \\ \vdots \\ F_{\mathcal{N}_{sc}} \end{bmatrix} m\frac{T_c}{\mathcal{N}_{sc}}\right) \quad (2)$$

[2]Note that the symbol period at point B is T_{cs} and symbol period at point A is $\frac{T_{cs}}{\mathcal{N}_{sc}}$.

[3]The use of PN-code is just a representative example of how we can integrate a modulation scheme with antenna array geometry. Note that instead of a PN-code we can use a Hadamard/Walsh sequence, or a chirp-pulse signal.

where $\mathrm{j} = \sqrt{-1}$ and the parameter $F_j = (j-1)\Delta F$ is the frequency offset of the j-th subcarrier from the main carrier frequency F_c and $\Delta F = \frac{1}{T_c}$ is the subcarrier spacing. Note that the proposed model is also applicable to a single carrier system as well as for a signal copy scheme instead of demultiplexing. Thus, at point D and for the $(\mathcal{N}_c\mathcal{N}_{sc}n + m)$-th interval, the transmitted vector is $\underline{a}_i[n]\,\alpha_i\left[\left\lceil\frac{m}{\mathcal{N}_{sc}}\right\rceil\right] \odot \underline{F}[m]$. Following this, the transmitter weight matrix of the i-th user $\overline{\mathbb{W}}_i \in C^{\overline{N}\times\mathcal{N}_{sc}}$, i.e.

$$\overline{\mathbb{W}}_i = \left[\overline{w}_{i1}, \overline{w}_{i2}, \ldots, \overline{w}_{i\mathcal{N}_{sc}}\right], \quad (3)$$

is applied on the modulated and spread data stream vector, at point D of Fig 2, to steer all the sub-carriers of the transmitter main lobe towards a desired DOA during the instant $(\mathcal{N}_c\mathcal{N}_{sc}n + m)$, yielding $\overline{\mathbb{W}}_i\left(\underline{a}_i[n]\,\alpha_i\left[\left\lceil\frac{m}{\mathcal{N}_{sc}}\right\rceil\right] \odot \underline{F}[m]\right)$ (see point E). Note that, the transmitter weights $\overline{w}_{ij}$ may be designed based on the feedback from the receiver. The design of these transmitter weights is out of the scope of this paper. The sequence of samples of the n-th symbol of the i-th user, obtained at point D, can be written in the form of a matrix $\mathbb{M}_i[n]$ given by

$$\mathbb{M}_i[n] = \left(\underline{a}_i[n] \otimes \left(\underline{c}_i \otimes \underline{1}_{\mathcal{N}_{sc}}\right)^T\right) \odot \mathbb{F}[n] \in \mathcal{C}^{\mathcal{N}_{sc}\times\mathcal{N}_c\mathcal{N}_{sc}}, \quad (4)$$

where the matrix $\mathbb{F}[n] \in C^{\mathcal{N}_{sc}\times\mathcal{N}_c\mathcal{N}_{sc}}$ represents the discretised points of the subcarrier vector, namely $\exp\left(\mathrm{j}2\pi[F_1, \ldots, F_{\mathcal{N}_{sc}}]^T t\right)$, at the time instants $t = \left\{(n\mathcal{N}_c\mathcal{N}_{sc} + 1)\frac{T_c}{\mathcal{N}_{sc}}, \ldots, (n+1)\mathcal{N}_c\mathcal{N}_{sc}\frac{T_c}{\mathcal{N}_{sc}}\right\}$, and

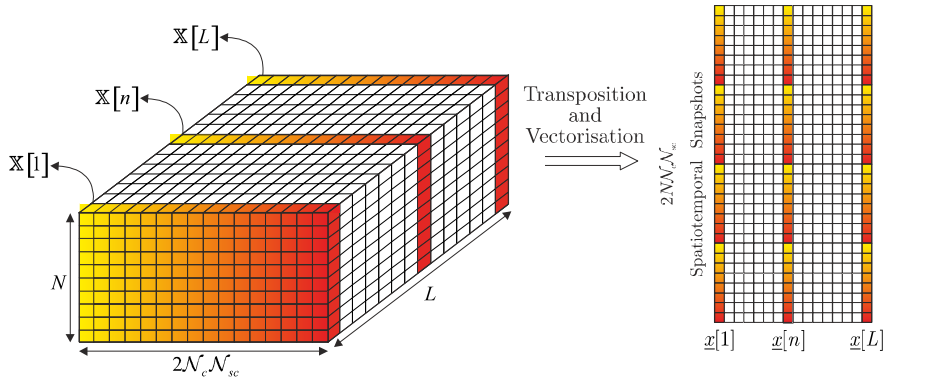

(a) 3D data cube matrix at the output of the TDLs

(b) Vectorisation of the 3D data cube matrix

Fig. 3: The 3D data cube and its vectorisation to form the spatiotemporal snapshot $\underline{x}[n]$.

is given by

$$\mathbb{F}[n] = [\underline{F}[n\mathcal{N}_c\mathcal{N}_{sc}+1], \ldots, \underline{F}[(n+1)\mathcal{N}_c\mathcal{N}_{sc}]. \quad (5)$$

Finally, the $\left(\overline{N}\times 1\right)$ message signal vector obtained at the output of the digital to analog (D/A) convertor (see point F) is transmitted onto the Tx antenna array of $\overline{N}$ antennas.

B. Channel Model Based on Tx and Rx Manifold Vectors

The channel, which is illustrated in Fig 2 (from point F to G), is assumed to be a frequency selective arrayed MIMO channel, as suited to mm-wave, and stationary over a small interval of L spatiotemporal snapshots. The subscripts i, k and j are used to represent the user, multipath and subcarrier respectively (i-th user, k-th multipath and j-th subcarrier).

Suppose that the transmitted signal from the i-th user arrives at the receiver via K_i paths. As illustrated in Fig 2, the branch of the channel which represents the k-th path, j-th subcarrier of the i-th user, is modelled with the Tx and Rx antenna array manifold vectors $\overline{\underline{S}}_{ikj} \in \mathcal{C}^{\overline{N}\times 3}$ and $\underline{S}_{ikj} \in \mathcal{C}^{N\times 3}$ respectively, a Doppler frequency shift $\mathcal{F}_{ikj}$ and path fading coefficient β_{ikj}. The parameter τ_{ik} denotes the time delay from the reference points of the Tx array to the Rx array.

The Rx antenna array manifold vector also known as spatial array manifold vector for the k-th path of the i-th user on the j-th subcarrier is defined as [17]:

$$\begin{aligned}\underline{S}_{ikj} &= \underline{S}(\theta_{ik}, \phi_{ik}, F_j) \\ &= \exp\left(-\mathrm{j}2\pi\frac{F_c+F_j}{c}[\underline{r}_x, \underline{r}_y, \underline{r}_z]\underline{u}(\theta_{ik}, \phi_{ik})\right), \quad (6)\end{aligned}$$

where $[\underline{r}_x, \underline{r}_y, \underline{r}_z] \in \mathcal{R}^{N\times 3}$ are the Cartesian coordinates of the receiver antenna array in metres, c is the speed of light and $\underline{u}(\theta_{ik}, \phi_{ik})$ points towards the direction of propagation

$$\underline{u}(\theta_{ik}, \phi_{ik}) \triangleq [\cos\theta_{ik}\cos\phi_{ik}, \sin\theta_{ik}\cos\phi_{ik}, \sin\phi_{ik}]^T, \quad (7)$$

with (θ_{ik}, ϕ_{ik}) denoting (azimuth, elevation) representing the DOA of the k-th path. Similarly, using $\overline{(\cdot)}$, i.e. a "bar" at the top of a symbol, to denote all equivalent parameters associated with the transmit array $[\overline{\underline{r}}_x, \overline{\underline{r}}_y, \overline{\underline{r}}_z] \in \mathcal{R}^{\overline{N}\times 3}$, the transmit array manifold vector is denoted by

$$\overline{\underline{S}}_{ikj} \triangleq \overline{\underline{S}}(\overline{\theta}_{ik}, \overline{\phi}_{ik}, F_j) \quad (8)$$

with $\left(\overline{\theta}_{ik}, \overline{\phi}_{ik}\right)$ representing the direction of departure (DOD) of the k-th path of the i-th user. With reference to point G in Fig 2, the $N\times 1$ baseband signal at the Rx antenna array can be modelled as follows

$$\begin{aligned}\underline{x}(t) = \sum_{i=1}^{M}\sum_{k=1}^{K_i}\sum_{j=1}^{\mathcal{N}_{sc}} &\beta_{ikj}\exp\left(\mathrm{j}2\pi\mathcal{F}_{ikj}t\right)\underline{S}_{ikj} \\ &\times \overline{\underline{S}}_{ikj}^H\overline{\underline{w}}_{ij}m_{ij}\left(t-\tau_{ik}\right) + \underline{\mathrm{n}}\left(t\right), \quad (9)\end{aligned}$$

where for the i-th user, j-th subcarrier and k-th path, the parameters β_{ikj}, $\mathcal{F}_{ikj}$ and τ_{ik} represent the complex path fading coefficient, the Doppler frequency and relative multipath delay respectively where

$$\mathcal{F}_{ikj} = -\frac{(F_c+F_j)\,v_{ik}}{c}, \quad (10)$$

with v_{ik} being the radial velocity of the i-th user's k-th path. The radial velocity is measured with respect to the Rx array reference point (i.e. $[0,0,0]$ Cartesian coordinate system). Note that the positive value of the radial velocity represents the same direction as $\underline{u}$. This is true for any relative motion in the wave propagation's path between Tx and Rx that changes the path's direction (i.e. radial velocity). In Equ 9, $m_{ij}\left(t\right)$ is the transmitted baseband message by the i-th user on the j-th subcarrier at time t. Furthermore, $\underline{\mathrm{n}}(t)$ is additive circular white Gaussian noise of zero mean and covariance matrix $\sigma_{\mathrm{n}}^2\mathbb{I}_N$, where σ_{n}^2 denotes the unknown noise power. In this paper, with no loss of generality, the users are assumed to be located in the (x,y) plane that is, zero elevation angles, i.e. $\phi_{ik} = \overline{\phi}_{ik} = 0\ \forall i,k$. The parametric model described helps in expressing the received antenna array signal vector $\underline{x}(t)$ (and its associated 2nd order statistics) as a function of the channel parameters (as shown in Equ 9) and consequently enables the design of very powerful channel estimators and receiver/beamformers.

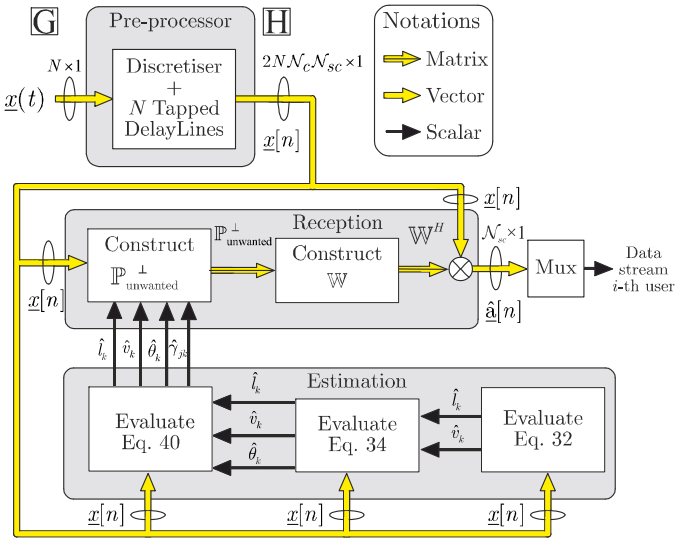

Fig. 4: Block diagram of the preprocessor consisting of the discretiser and TDLs, followed by the channel estimator and the STAR-subspace receiver. Please note that the subscript i has been set to one and hence has been ignored.

C. Receiver Model

The received signal $\underline{x}(t)$, which is shown at point G in Fig 2 and Fig 4, is fed to a preprocessor consisting of a discretiser of a sampling period $T_s = \frac{T_c}{\mathcal{N}_{sc}}$ and a bank of N tapped delay lines (TDLs) of length $2\mathcal{N}_c\mathcal{N}_{sc}$. Since, the generic case of asynchronous systems is considered, the transmitted data symbols do not arrive at the antennas at the beginning of their interval but with a relative delay. Thus, during the nT_{cs} period, the TDLs contain the contribution of the n-th Tx symbol plus some information of the previous $(n-1)$ and next $(n+1)$ symbols. In this paper, we use the term inter symbol interference (ISI) to represent this contribution arising from this preprocessor. Figure 3a shows the 3D data cube which represents the received discretised signal, where the n-th slice of the data cube matrix is of size $N \times 2\mathcal{N}_c\mathcal{N}_{sc}$ corresponding to the data stored in the bank of TDLs at the nT_{cs} period. The vectorisation of the transposed n-th data slice provides the n-th spatiotemporal snapshot $\underline{x}[n]$ $\in C^{2N\mathcal{N}_c\mathcal{N}_{sc}\times 1}$ as shown in Fig 3b. Hence, the output $\underline{x}[n]$ at point H in Fig 4 can be written as

$$\underline{x}[n] = \mathrm{vec}\left(\mathbb{X}^T[n]\right), \tag{11}$$

and this section presents the mathematical model of the same. Thus, the vector $\underline{x}[n]$ contains the n-th symbol of the desired user along with ISI, MAI and noise effects. In order to model these contributions, for the i-th user, j-th subcarrier and k-th path, the concept of the array manifold vector is extended to the Doppler-spatiotemporal array (Doppler-STAR) manifold vector $\underline{\mathfrak{h}}_{ikj} \in \mathcal{C}^{2N\mathcal{N}_c\mathcal{N}_{sc}\times 1}$ [18] given as follows

$$\underline{\mathfrak{h}}_{ikj} = \underline{S}_{ikj} \otimes \left(\mathbb{J}^{l_{ik}}\underline{\mathfrak{a}}_j\left[l_{ik}\right] \odot \underline{\mathcal{F}}_{ikj}\right) = \mathbb{A}_{ikj}\underline{S}_{ikj}, \tag{12}$$

where $\mathbb{A}_{ikj} \in C^{2N\mathcal{N}_c\mathcal{N}_{sc}\times N}$ is the linear mapping between the space-only manifold vector $\underline{S}_{ikj}$ and the Doppler-STAR manifold vector $\underline{\mathfrak{h}}_{ikj}$ defined as

$$\mathbb{A}_{ikj} = \mathbb{I}_N \otimes \left(\mathbb{J}^{l_{ik}}\underline{\mathfrak{a}}_j\left[l_{ik}\right] \odot \underline{\mathcal{F}}_{ikj}\right). \tag{13}$$

The matrix $\mathbb{J}$ (or $\mathbb{J}^T$) is a $2\mathcal{N}_c\mathcal{N}_{sc} \times 2\mathcal{N}_c\mathcal{N}_{sc}$ matrix and the power l of $\mathbb{J}$ (or $\mathbb{J}^T$) when applied to a vector $\underline{x}$, i.e. $\mathbb{J}^l\underline{x}$ (or $\left(\mathbb{J}^T\right)^l\underline{x}$), downshifts (or upshifts) the vector $\underline{x}$ by l elements and is given as follows

$$\mathbb{J} = \begin{bmatrix} \underline{0}^T_{2\mathcal{N}_c\mathcal{N}_{sc}-1} & 0 \\ \mathbb{I}_{2\mathcal{N}_c\mathcal{N}_{sc}-1} & \underline{0}_{2\mathcal{N}_c\mathcal{N}_{sc}-1} \end{bmatrix}. \tag{14}$$

In Equ 12, the parameter $l_{ik} = \left\lfloor \frac{\tau_{ik}}{T_s} \right\rfloor \bmod \mathcal{N}_c\mathcal{N}_{sc}$ stands for the discrete relative path delay. Also, the vector $\underline{\mathfrak{a}}_j[l_{ik}] \in \mathcal{C}^{2\mathcal{N}_c\mathcal{N}_{sc}\times 1}$ that incorporates the temporal variation is defined as follows

$$\underline{\mathfrak{a}}_{ikj} \triangleq \underline{\mathfrak{a}}_j[l_{ik}] = \left(\begin{bmatrix} \underline{c}_i \\ \underline{0}_{\mathcal{N}_c} \end{bmatrix} \otimes \underline{1}_{\mathcal{N}_{sc}}\right) \odot \begin{bmatrix} \exp(\mathrm{j}2\pi F_j\left(0 - l_{ik}\right)T_s) \\ \exp(\mathrm{j}2\pi F_j\left(1 - l_{ik}\right)T_s) \\ \vdots \\ \exp(\mathrm{j}2\pi F_j\left(\mathcal{N}_c\mathcal{N}_{sc} - 1 - l_{ik}\right)T_s) \\ \underline{0}_{\mathcal{N}_c\mathcal{N}_{sc}} \end{bmatrix}. \tag{15}$$

The temporal variation within a symbol arising from the Doppler frequency shift is modelled as the vector $\underline{\mathcal{F}}_{ikj} \in \mathcal{C}^{2\mathcal{N}_c\mathcal{N}_{sc}\times 1}$ written as

$$\underline{\mathcal{F}}_{ikj} = \exp\left(\mathrm{j}\left[0, 1, \ldots, 2\mathcal{N}_c\mathcal{N}_{sc} - 1\right]^T 2\pi\mathcal{F}_{ikj}T_s\right). \tag{16}$$

Using the Doppler-STAR manifold vector defined in Equ 12, we can model the n-th spatiotemporal snapshot $\underline{x}[n]$ as follows

$$\underline{x}[n] = \sum_{i=1}^{M}\sum_{j=1}^{\mathcal{N}_{sc}}\left[\mathbb{H}_{ij}, \mathbb{H}^{\mathrm{comb}}_{ij}\right] \times \begin{bmatrix} \left(\underline{\gamma}_{ij} \odot \underline{f}_{ij}[n]\right)\mathrm{a}_{ij}[n] \\ \left(\underline{\gamma}_{ij} \odot \underline{f}_{ij}[n-1]\right)\mathrm{a}_{ij}[n-1] \\ \left(\underline{\gamma}_{ij} \odot \underline{f}_{ij}[n+1]\right)\mathrm{a}_{ij}[n+1] \end{bmatrix} + \underline{\mathrm{n}}[n], \tag{17}$$

where $\mathrm{a}_{ij}[n]$ represents the symbol transmitted by the i-th user on the j-th subcarrier and $\underline{\mathrm{n}}[n]$ represents the sampled noise. Although subcarriers are employed, strictly speaking, we do not use the "frequency domain" as all the subcarriers are expressed in the time domain. Thus, the proposed approach belongs to the family of spatiotemporal techniques. Note that the above equations are simplified to the single carrier system by applying $\mathcal{N}_{sc} = 1$ and dropping the subscript j representing the subcarrier index (see Appendix A). The matrix $\mathbb{H}_{ij}$ contains the Doppler-STAR manifold vectors of all the multipaths of the j-th subcarrier of the i-th user, constructed as follows

$$\mathbb{H}_{ij} = [\underline{\mathfrak{h}}_{i1j}, \underline{\mathfrak{h}}_{i2j}, ..., \underline{\mathfrak{h}}_{iK_ij}] \in \mathcal{C}^{2N\mathcal{N}_c\mathcal{N}_{sc}\times K_i}. \tag{18}$$

In Equ 17, the matrix $\mathbb{H}^{\mathrm{comb}}_{ij} \in \mathcal{C}^{2N\mathcal{N}_c\mathcal{N}_{sc}\times 2K_i}$ contains

delayed versions of the matrix $\mathbb{H}_{ij}$ (ISI) and is defined as

$$\mathbb{H}_{ij}^{\text{comb}} = \left[(\mathbb{I}_N \otimes (\mathbb{J}^T)^{\mathcal{N}_c\mathcal{N}_{sc}})\mathbb{H}_{ij}, (\mathbb{I}_N \otimes (\mathbb{J})^{\mathcal{N}_c\mathcal{N}_{sc}})\mathbb{H}_{ij}\right]. \tag{19}$$

In addition, the vector $\underline{\gamma}_{ij}$ contains the path fading coefficients and the gain provided by transmit beamforming for all the multipaths of the j-th subcarrier of the i-th user. That is,

$$\underline{\gamma}_{ij} = \underline{\beta}_{ij} \odot \left[\overline{\underline{S}}_{j1}^H \overline{\underline{w}}_{ij}, \ldots, \overline{\underline{S}}_{jK_i}^H \overline{\underline{w}}_{ij}\right]^T, \tag{20}$$

where the vector $\underline{\beta}_{ij} \in \mathcal{C}^{K_i \times 1}$

$$\underline{\beta}_{ij} = [\beta_{i1j}, \beta_{i2j}, ..., \beta_{iK_ij}]^T, \tag{21}$$

contains the K_i multipath fading coefficients of the j-th subcarrier of the i-th user. Finally, the vector $\underline{f}_{ij}[n] \in \mathcal{C}^{K_i \times 1}$ incorporates the temporal variation of the subcarriers and Doppler shift from one symbol to the other, defined as

$$\underline{f}_{ij}[n] = \exp(\mathrm{j}2n\pi F_j T_{cs}) \exp\left(\mathrm{j}2n\pi \left[\mathcal{F}_{i1j}, \ldots, \mathcal{F}_{iK_ij}\right]^T T_{cs}\right). \tag{22}$$

Without any loss of generality, the first user is assumed to be the desired user, i.e. $i = 1$, and thus $\underline{x}[n]$ can be rewritten as follows to distinguish the desired signal, ISI, MAI and noise component

$$\begin{aligned}
\underline{x}[n] = &\overbrace{\sum_{j=1}^{\mathcal{N}_{sc}} \mathbb{H}_{1j}\left(\underline{\gamma}_{1j} \odot \underline{f}_{1j}[n]\right) \mathrm{a}_{1j}[n]}^{\text{Desired term}} \\
&+ \overbrace{\sum_{j=1}^{\mathcal{N}_{sc}} \mathbb{H}_{1j}^{\text{comb}} \begin{bmatrix} \left(\underline{\gamma}_{1j} \odot \underline{f}_{1j}[n-1]\right) \mathrm{a}_{1j}[n-1] \\ \left(\underline{\gamma}_{1j} \odot \underline{f}_{1j}[n+1]\right) \mathrm{a}_{1j}[n+1] \end{bmatrix}}^{\text{ISI term}} \\
&+ \overbrace{\sum_{i=2}^{M}\sum_{j=1}^{\mathcal{N}_{sc}} \left[\mathbb{H}_{ij}^{\text{comb}}, \mathbb{H}_{ij}\right] \begin{bmatrix} \left(\underline{\gamma}_{ij} \odot \underline{f}_{ij}[n-1]\right) \mathrm{a}_{ij}[n-1] \\ \left(\underline{\gamma}_{ij} \odot \underline{f}_{ij}[n+1]\right) \mathrm{a}_{ij}[n+1] \\ \left(\underline{\gamma}_{ij} \odot \underline{f}_{ij}[n]\right) \mathrm{a}_{ij}[n] \end{bmatrix}}^{\text{MAI term}} \\
&+ \overbrace{\underline{\mathrm{n}}[n]}^{\text{noise}}.
\end{aligned} \tag{23}$$

Based on Equ 23, the theoretical covariance matrix of the received signal $\mathbb{R}_{xx} \in \mathcal{C}^{2N\mathcal{N}_c\mathcal{N}_{sc} \times 2N\mathcal{N}_c\mathcal{N}_{sc}}$ can be written as

$$\begin{aligned}
\mathbb{R}_{xx} &= \mathcal{E}\{\underline{x}[n]\underline{x}^H[n]\} \\
&= \overbrace{\sum_{j=1}^{\mathcal{N}_{sc}} \mathbb{H}_{1j}\mathbb{G}_{1j}\mathbb{H}_{1j}^H}^{\text{Desired term}} + \overbrace{\sum_{j=1}^{\mathcal{N}_{sc}} \mathbb{H}_{1j}^{\text{comb}} \left(\mathbb{I}_2 \otimes \mathbb{G}_{1j}\right) \left(\mathbb{H}_{1j}^{\text{comb}}\right)^H}^{\triangleq \mathbb{R}_{\text{ISI}}} \\
&\quad + \overbrace{\sum_{i=2}^{M}\sum_{j=1}^{\mathcal{N}_{sc}} \left[\mathbb{H}_{ij}^{\text{comb}}, \mathbb{H}_{ij}\right] \left(\mathbb{I}_3 \otimes \mathbb{G}_{ij}\right) \left[\mathbb{H}_{ij}^{\text{comb}}, \mathbb{H}_{ij}\right]^H}^{\triangleq \mathbb{R}_{\text{MAI}}} \\
&\quad + \overbrace{\sigma_{\text{n}}^2 \mathbb{I}_{2N\mathcal{N}_c\mathcal{N}_{sc}}}^{\triangleq \mathbb{R}_{\text{nn}}},
\end{aligned} \tag{24}$$

where $\mathbb{G}_{ij} \in \mathcal{C}^{K_i \times K_i}$ represents the multipath power gain matrix given by

$$\begin{aligned}
\mathbb{G}_{ij} &= \mathcal{E}\left\{\left(\underline{\gamma}_{ij} \odot \underline{f}_{ij}[n]\right) \mathrm{a}_{ij}[n]\mathrm{a}_{ij}^*[n] \left(\underline{\gamma}_{ij} \odot \underline{f}_{ij}[n]\right)^H\right\} \\
&= \mathrm{diag}\left\{\underline{\gamma}_{ij} \odot \underline{\gamma}_{ij}^*\right\} \odot \mathcal{E}\left\{\underline{f}_{ij}[n]\underline{f}_{ij}^H[n]\right\} \\
&= \mathrm{diag}\left\{\underline{\gamma}_{ij} \odot \underline{\gamma}_{ij}^*\right\},
\end{aligned} \tag{25}$$

since $\mathcal{E}\left\{\mathrm{a}_{ij}[n]\mathrm{a}_{ij}^*[n]\right\} = 1$ and $\mathcal{E}\left\{\underline{f}_{ij}[n]\underline{f}_{ij}^H[n]\right\} = \mathbb{I}_{K_i}$. Note that, with the L spatiotemporal snapshots shown in Fig 3, the practical covariance matrix corresponding to the theoretical one given by Equ 24, can be obtained as follows

$$\mathbb{R}_{xx} = \frac{1}{L}\left[\underline{x}\left[1\right], \ldots, \underline{x}\left[L\right]\right]\left[\underline{x}\left[1\right], \ldots, \underline{x}\left[L\right]\right]^H. \tag{26}$$

D. Fundamental Performance Bounds

As stated in [17], the estimation performance of an arrayed system depends on the radius of the uncertainty sphere centered at the true value on the manifold. This uncertainty sphere arises due to the finite sampling effect characterised by the number of snapshots L and the SNR.

In the case of the Cramer-Rao bound (CRB), which gives a theoretical lower bound on the variance of the estimation error of the azimuth (θ) for a source, for space-only systems, it has been shown in [17] that

$$\mathrm{CRB}_{\text{space-only}}\left[\theta\right] = \frac{1}{2\left(\mathrm{SNR} \times L\right)\dot{s}^2\left(\theta\right)}. \tag{27}$$

Here $\dot{s}\left(\theta\right) = \frac{\partial s}{\partial \theta}$ denotes the rate of change of the arc length s of the array manifold and it is a function of the array geometry. For instance for linear arrays of N sensors, $\dot{s}\left(\theta\right) = \pi \left\|\underline{r}_x\right\| \sin\theta$.

However, to evaluate the CRB for the spatiotemporal system employed in this paper, Equ 27 needs to be extended to incorporate the Doppler-STAR manifold vector. The rate of change of the arc length of the extended manifold $\dot{s}_{\mathcal{H}}\left(\theta\right)$ has been derived in [18] as

$$\dot{s}_{\mathcal{H}}\left(\theta\right) = \sqrt{\sigma_{\dot{\mathbb{A}}}^2 \dot{s}^2\left(\theta\right) + \sigma_{\mathbb{A}}^2 N}, \tag{28}$$

where $\sigma_{\mathbb{A}}^2$ and $\sigma_{\dot{\mathbb{A}}}^2$ are defined as follows

$$\sigma_{\mathbb{A}}^2 = \frac{\mathrm{Tr}\left\{\mathbb{A}^H\mathbb{A}\right\}}{N} \text{ and } \sigma_{\dot{\mathbb{A}}}^2 = \frac{\mathrm{Tr}\left\{\dot{\mathbb{A}}^H\dot{\mathbb{A}}\right\}}{N}. \tag{29}$$

Using Equ 13 in conjunction with Equ 29, the following can be obtained

$$\sigma_{\mathbb{A}}^2 = \mathcal{N}_c\mathcal{N}_{sc} \text{ and } \sigma_{\dot{\mathbb{A}}}^2 = 0 \overset{\text{Equ 28}}{\Longrightarrow} \dot{s}_{\mathcal{H}}\left(\theta\right) = \sqrt{\mathcal{N}_c\mathcal{N}_{sc}}\dot{s}\left(\theta\right). \tag{30}$$

Using this in conjunction with Equ 27, we can derive the CRB of the proposed spatiotemporal system as follows

$$\boxed{\mathrm{CRB}_{\text{Doppler-STAR}}\left[\theta\right] = \frac{1}{\mathcal{N}_c\mathcal{N}_{sc}}\mathrm{CRB}_{\text{space-only}}\left[\theta\right].} \tag{31}$$

This illustrates that, for the same number of antennas, the proposed spatiotemporal system outperforms the corresponding space-only system in terms of the estimation error. Remember that θ is now one of the unknown wireless channel parameters

which should be estimated and this will be presented in the following section.

III. Proposed Spatiotemporal Beamformer Design

Based on the 3D data cube shown in Fig 3 and the spatiotemporal snapshot $\underline{x}[n]$ modelled by Equ 23, in this section, a novel spatiotemporal beamformer is proposed for the millimetre wave communication system described previously. As shown in Fig 4, this beamformer consists of a Doppler-spatiotemporal array (STAR)-subspace receiver utilising the estimated parameters, denoted by $\widehat{(\cdot)}$, from a novel channel estimator. The design of these blocks is discussed in the next few sections. Without any loss of generality, the first user is considered to be the desired user and for notational convenience the subscript i is dropped.

Based on Equs 23 and 26, the following parameters of interest of all the paths of the desired user across all subcarriers should be estimated: relative multipath delay, channel fading coefficients, Doppler frequency and DOA. Note that the estimation of Doppler frequency corresponding to a path and subcarrier is equivalent to the estimation of radial velocity for the same. As shown in the estimation block of Fig 4, this complex estimation problem is broken down into smaller units of lower complexity. The search procedures are carried out in the baseband. Firstly, the delay and radial velocity are jointly estimated, followed by the estimation of DOA. Then, the combined contribution of the channel fading coefficients and transmit beamforming weights is estimated. These estimation procedures are blind and based on the assumptions of plane-wave propagation, known array geometry and fully calibrated arrays. The proposed framework utilises

(i) the extended array manifold which is a mathematical object embedded in a multidimensional complex space that entirely characterizes an antenna array (of a given geometry) for the whole set of values in the parameter space,

(ii) the preprocessed received array data, and in particular its second order statistics, which can provide a linear space spanned by the signals (signal subspace),

where the solution of the estimation problem is the intersection of the non-linear subspace-(i) and the linear subspace-(ii). This intersection can be found by the 2D and 1D search procedures to yield the K paths of the desired user as described in the Sections III-A and III-B below.

A. Joint Delay-Velocity Estimation

In this first stage of joint estimation of delay and velocity, since the DOA is unknown, the spatial dimension provided by the N antennas cannot be exploited. Hence, the subspace is reduced from $2N\mathcal{N}_c\mathcal{N}_{sc}$ to $2\mathcal{N}_c\mathcal{N}_{sc}$ dimensions by a simple rearrangement of the slices $\mathbb{X}[n]$ of the 3D data cube discussed in Section II-C. Using the eigendecomposition of the covariance of the rearranged matrix $\left[\mathbb{X}^T[1],\ldots,\mathbb{X}^T[n],...,\mathbb{X}^T[L]\right] \in \mathcal{C}^{2\mathcal{N}_c\mathcal{N}_{sc}\times NL}$, the projection on the noise subspace $\mathbb{P}_{\mathrm{n}}$ is obtained. Note that, although the number of dimensions is reduced, increased number of snapshots are obtained due to the format of the rearrangement. The parameters corresponding to the desired user will lie in the signal subspace spanned by the temporal part of the manifold vector in Equ 12, given by $\mathbb{J}^{l_k}\underline{\mathfrak{a}}_{kj}\odot\underline{\mathcal{F}}_{kj}$, containing the PN code of the desired user and a Doppler component. Using the fact that this subspace is orthogonal to the estimated noise subspace $\mathbb{P}_n$, the cost function $\xi(l_k,v_k)$ estimates the delay-velocity jointly for the k-th multipath and can be defined as follows

$$\xi\left(l_k,v_k\right)=\frac{1}{\mathcal{N}_{sc}}\sum_{j=1}^{\mathcal{N}_{sc}}\frac{\left(\mathbb{J}^{l_k}\underline{\mathfrak{a}}_{kj}\odot\underline{\mathcal{F}}_{kj}\right)^H\left(\mathbb{J}^{l_k}\underline{\mathfrak{a}}_{kj}\odot\underline{\mathcal{F}}_{kj}\right)}{\left(\mathbb{J}^{l_k}\underline{\mathfrak{a}}_{kj}\odot\underline{\mathcal{F}}_{kj}\right)^H\mathbb{P}_{\mathrm{n}}\left(\mathbb{J}^{l_k}\underline{\mathfrak{a}}_{kj}\odot\underline{\mathcal{F}}_{kj}\right)}, \tag{32}$$

where

$$\begin{aligned}\underline{\mathcal{F}}_{kj}&\triangleq\underline{\mathcal{F}}_{kj}\left(v_k\right)\\&=\exp\left(\mathrm{j}\left[0,1,\ldots,2\mathcal{N}_c\mathcal{N}_{sc}-1\right]^T\frac{2\pi\left(F_c+F_j\right)v_kT_s}{c}\right).\end{aligned} \tag{33}$$

The peaks obtained from the 2-dimensional search using this cost function over a 2D grid (spanning the range of possible values of delay and velocity) yield the delay and velocity values corresponding to the multipaths of the desired user. The number of evaluations is not a function of the number of antennas but depends purely on the chosen 2D grid. Furthermore, the evaluations are independent from each other and can be done in parallel. Note that, for the multicarrier system, a combined estimate of all subcarriers is evaluated which can help combat frequency selective fades in the mm-wave channel.

B. DOA Estimation

The design of this cost function follows the logic stated previously that the intersection of the noise subspace spanned by $\mathbb{P}_{\mathrm{n}}$ and the extended Doppler-STAR manifold object will yield the set of all Doppler-STAR manifold vectors $\underline{\mathfrak{h}}_j$ (see Equ 12) of the desired user's paths. Hence, for $k=1,...,K$ pairs of estimated $\left(\widehat{l}_k,\widehat{v}_k\right)$, a 1D search is carried out over the space-time cost function given by

$$\xi\left(\theta_{\widehat{l}_k,\widehat{v}_k}\right)=\frac{1}{\mathcal{N}_{sc}}\sum_{j=1}^{\mathcal{N}_{sc}}\frac{\underline{\mathfrak{h}}_j^H\left(\theta_{\widehat{l}_k,\widehat{v}_k}\right)\underline{\mathfrak{h}}_j\left(\theta_{\widehat{l}_k,\widehat{v}_k}\right)}{\underline{\mathfrak{h}}_j^H\left(\theta_{\widehat{l}_k,\widehat{v}_k}\right)\mathbb{P}_{\mathrm{n}}\underline{\mathfrak{h}}_j\left(\theta_{\widehat{l}_k,\widehat{v}_k}\right)}, \tag{34}$$

where $\mathbb{P}_{\mathrm{n}}$ represents the projection on the noise subspace obtained from the eigendecomposition of the covariance matrix $\mathbb{R}_{xx}$.

C. Combined Fading Coefficient Estimation

Post estimating the delay, radial velocity and DOA, the residual combined parameter γ_{kj} to be estimated consists of the complex path fading coefficient and the transmit beamforming gain for the j-th subcarrier and k-th path. In this section, a near-far algorithm to estimate the amplitude and phase of γ_{kj} is described. The steps in the algorithm are as follows:

1) The subspace $\mathbb{R}_{kj,\mathrm{un}}$ consisting of MAI, noise and the other $K-1$ paths of the desired user is constructed

by subtracting the effects of $\hat{\underline{\mathfrak{h}}}_{kj}$ (estimated in Sections III-A and III-B) from the data covariance matrix

$$\mathbb{R}_{kj,\mathrm{un}} = \mathbb{R}_{xx} - \left\|\hat{\gamma}_{kj}\right\|^2 \hat{\underline{\mathfrak{h}}}_{kj}\hat{\underline{\mathfrak{h}}}_{kj}^H, \tag{35}$$

where $\left\|\hat{\gamma}_{kj}\right\|$ can be estimated using the following cost function inspired from [19]

$$\left\|\hat{\gamma}_{kj}\right\| = \arg\min_{\|\gamma\|} \xi_{kj}\left(\|\gamma\|\right), \tag{36}$$

where

$$\xi_{kj}\left(\|\gamma\|\right) = \sum_{\substack{m=1 \\ \mathrm{eig}_m>0}}^{2N\mathcal{N}_c\mathcal{N}_{sc}} \left(1+\mathrm{eig}_m\left(\mathbb{R}_{kj}\left(\|\gamma\|\right)\right)\right) + 10\log_{10}\left(\sum_{\substack{m=1 \\ \mathrm{eig}_m<0}}^{2N\mathcal{N}_c\mathcal{N}_{sc}} \left|\mathrm{eig}_m\left(\mathbb{R}_{kj}\left(\|\gamma\|\right)\right)\right|\right), \tag{37}$$

with

$$\mathbb{R}_{kj}\left(\|\gamma\|\right) = \mathbb{R}_{xx} - \mathrm{eig}_{\min}\left(\mathbb{R}_{xx}\right) - \|\gamma\|_{kj}^2\, \hat{\underline{\mathfrak{h}}}_{kj}\hat{\underline{\mathfrak{h}}}_{kj}^H. \tag{38}$$

(Note that the aforementioned 1D cost function of Equ 37 is searched for the amplitude $\|\gamma\|$ that reduces the rank of the received signal covariance matrix $\mathbb{R}_{xx}$ by one.) By partitioning the space spanned by the columns of $\mathbb{R}_{kj,\mathrm{un}}$ into "unwanted" signal subspace and "noise" subspace, the projection operator $\mathbb{P}_{kj,\mathrm{un}}$ is formed using the eigenvectors corresponding to the "unwanted signal". This, in turn, can be utilised to construct $\mathbb{P}^{\perp}_{kj,\mathrm{un}}$ to isolate the j-th subcarrier and k-th path of the desired user and remove the unwanted signals, that is

$$\mathbb{P}^{\perp}_{kj,\mathrm{un}} = \mathbb{I}_{2N\mathcal{N}_c\mathcal{N}_{sc}} - \mathbb{P}_{kj,\mathrm{un}}. \tag{39}$$

2) By exploiting the noise tolerance of the modulation and utilising all the available symbols in the observation interval of L snapshots, the phase of $\hat{\gamma}_{kj}$ can be estimated as follows

$$\angle\hat{\gamma}_{kj} = \left\{\frac{1}{L}\sum_{n=1}^{L}\left\{\angle\left(f_{kj}^*[n]\hat{\underline{\mathfrak{h}}}_{kj}^H\mathbb{P}^{\perp}_{kj,\mathrm{un}}\underline{x}[n]\right) - \hat{\gamma}_{kj,\mathrm{gu}}\right\}\bmod\psi - \psi_0\right\} + \angle\hat{\gamma}_{kj,\mathrm{gu}}, \tag{40}$$

where $\angle\hat{\gamma}_{kj,\mathrm{gu}}$ is an initial guess of $\angle\hat{\gamma}_{kj}$ obtained with the help of $\mathbb{P}^{\perp}_{kj,\mathrm{un}}$ as below

$$\angle\hat{\gamma}_{kj,\mathrm{gu}} = \angle\mathrm{a}_j^*[1]\hat{\underline{\mathfrak{h}}}_{kj}^H\left(\mathbb{P}^{\perp}_{kj,\mathrm{un}}\underline{x}[1]\right). \tag{41}$$

Here $\mathrm{a}_j[1]$ is the first symbol on the j-th subcarrier of every observation interval which is assumed to be the header (i.e. known). There are two important points to be noted here. Firstly, the role of $\mathbb{P}^{\perp}_{kj,\mathrm{un}}$ is to make the procedure near-far resistant. Secondly, after suppressing the interference, two levels of noise suppression are utilised. First level of obtaining $\angle\hat{\gamma}_{kj,\mathrm{gu}}$ relies on the inherent noise tolerance of the modulation while the second level uses an maximum likelihood (ML) averaging approach to obtain an improved estimate of the phase. Note that this is under the assumption that the phase deviation introduced by the noise is within $\pm\psi$ where ψ is the minimum phase difference between two constellation points and ψ_0 is the initial modulation angle in the chosen modulation scheme.

Please note that the above proposed near-far resistant estimation procedure for the phase of the desired parameter γ is one of the novelties of this paper.

D. Design of the Rx Spatiotemporal Beamformer Weights

In this subsection, the estimated channel parameters are employed to construct spatiotemporal beamforming weights to steer very high gain towards the directions of interest. We present a novel single-user Doppler-STAR-subspace receiver that explicitly cancels ISI and MAI and utilises the multipath effects in a frequency selective channel constructively. The steps to build these weights for the j-th subcarrier are as follows:

1) As a first step, the unwanted subspace (or the subspace perpendicular to the j-th subcarrier) $\widehat{\mathbb{R}}_{\mathrm{unwanted}}$ is required to be estimated. Towards this, the contribution of the desired user to the received signal covariance matrix, namely $\widehat{\mathbb{R}}_{\mathrm{des}}$, has to be removed from the received signal covariance matrix $\mathbb{R}_{xx}$. However, in order to receive the data on the j-th subcarrier, the contribution of the other subcarriers is required to be suppressed from $\widehat{\mathbb{R}}_{\mathrm{des}}$ and made a part of the estimated interference subspace given by
$$\widehat{\mathbb{R}}_{\mathrm{unwanted}} = \mathbb{R}_{xx} - \widehat{\mathbb{H}}_j\widehat{\mathbb{G}}_j\widehat{\mathbb{H}}_j^H. \tag{42}$$
2) By performing the eigendecomposition of the estimated $\widehat{\mathbb{R}}_{\mathrm{unwanted}}$, the matrix $\mathbb{E}_{\mathrm{s}}$ whose columns contain the eigenvectors spanning the corresponding unwanted signal subspace can be obtained. Using this matrix $\mathbb{E}_{\mathrm{s}}$, a projection operator orthogonal to the MAI, ISI and other subcarriers may be built as follows
$$\mathbb{P}^{\perp}_{j,\mathrm{unwanted}} = \mathbb{I}_{2N\mathcal{N}_c\mathcal{N}_{sc}} - \mathbb{E}_{\mathrm{s}}\left(\mathbb{E}_{\mathrm{s}}^H\mathbb{E}_{\mathrm{s}}\right)^{-1}\mathbb{E}_{\mathrm{s}}^H. \tag{43}$$
3) The projection operator from step 2 is used to form the Doppler-STAR-subspace weights as
$$\underline{w}_{j,\mathrm{sub}} = \mathbb{P}^{\perp}_{j,\mathrm{unwanted}}\widehat{\mathbb{H}}_j\left(\widehat{\mathbb{H}}_j^H\mathbb{P}^{\perp}_{j,\mathrm{unwanted}}\widehat{\mathbb{H}}_j\right)^{-1}\widehat{\underline{\gamma}}_j. \tag{44}$$

An estimate of the transmitted symbol vector $\widehat{\underline{\mathrm{a}}}[n]$ (point B in Fig 2) is formed as

$$\widehat{\underline{\mathrm{a}}}[n] = \mathbb{W}^H\underline{x}[n], \tag{45}$$

with $\mathbb{W}$ being the concatenation of the Doppler-STAR-subspace weights designed for all the subcarriers that is

$$\mathbb{W} = \left[\underline{w}_1, \ldots, \underline{w}_{\mathcal{N}_{sc}}\right] \in \mathcal{C}^{2N\mathcal{N}_c\mathcal{N}_{sc}\times\mathcal{N}_{sc}}. \tag{46}$$

For the sake of completeness, the performance of this receiver is compared to two other extensively used receivers: (a) single-user Doppler-STAR-RAKE receiver and (b) multi-user Doppler-STAR-decorrelating receiver. The weights for the

$$[\overline{r}_x, \overline{r}_y, \overline{r}_z]^T =$$

$$\begin{bmatrix} 2.56, & 2.37, & 1.81, & 0.98, & 0.00, & -0.98, & -1.81, & -2.37, & -2.56, & -2.37, & -1.81, & -0.98, & 0.00, & 0.98, & 1.81, & 2.37 \\ 0.00, & 0.98, & 1.81, & 2.37, & 2.56, & 2.37, & 1.81, & 0.98, & 0.00, & -0.98, & -1.81, & -2.37, & -2.56, & -2.37, & -1.81, & -0.98 \\ 0.00, & 0.00, & 0.00, & 0.00, & 0.00, & 0.00, & 0.00, & 0.00, & 0.00, & 0.00, & 0.00, & 0.00, & 0.00, & 0.00, & 0.00, & 0.00 \end{bmatrix} \tag{50}$$

$$[\underline{r}_x, \underline{r}_y, \underline{r}_z]^T = \begin{bmatrix} 1.43, & 0.90, & -0.05, & -0.98, & -1.45, & -1.24, & -0.45, & 0.55, & 1.29 \\ 0.30, & 1.15, & 1.46, & 1.09, & 0.20, & -0.77, & -1.39, & -1.36, & -0.69 \\ 0.00, & 0.00, & 0.00, & 0.00, & 0.00, & 0.00, & 0.00, & 0.00, & 0.00 \end{bmatrix} \tag{51}$$

Doppler-STAR-RAKE receiver are given as

$$\underline{w}_{j,\mathrm{RAKE}} = \widehat{\mathbb{H}}_j \widehat{\underline{\gamma}}_j. \tag{47}$$

The multiuser Doppler-STAR-decorrelating receiver (zero-forcing receiver) exploits the knowledge of the entire channel (i.e. all users) given by

$$\mathbb{H} = \left[\mathbb{H}_{11}^{\mathrm{comb}}, \mathbb{H}_{11}, \ldots, \mathbb{H}_{M\mathcal{N}_{sc}}^{\mathrm{comb}}, \mathbb{H}_{M\mathcal{N}_{sc}}\right], \tag{48}$$

where $\mathbb{H}_{ij}$ represents the contribution of the j-th subcarrier of the i-th user. The version of this receiver introduced in [20] as been employed here, expressed as

$$\underline{w}_{j,\mathrm{dec}} = \mathrm{col}_{3jK_1-K_1+1:3jK_1} \left\{ \left[\mathbb{H} \left(\mathbb{H}^H \mathbb{H} \right)^{-1} \right] \right\} \widehat{\underline{\gamma}}_j, \tag{49}$$

where the notation $\mathrm{col}_{3jK_1-K_1+1:3jK_1}$ has been used to indicate that the $(3jK_1 - K_1 + 1)$-th to $(3jK_1)$-th columns are extracted.

IV. Computer Simulation Studies

To evaluate the performance of the proposed spatiotemporal beamformer and the associated parameter estimator, computer simulation studies have been performed. Without any loss of generality, both the Tx and Rx antenna arrays are considered to be uniform circular arrays (UCA) of 16 and 9 elements respectively lying in the (x, y) plane. The Cartesian coordinates of the elements of these two arrays are indicated in $\left(\frac{\lambda}{2} \text{ units}\right)$ in Equ 50 and Equ 51 respectively.

The simulation parameters have been chosen to match the environment of the future 5G system. Empirical studies indicate that at millimetre wave frequencies, due to high path loss and scattering, only a few significant multipaths may be present with the LOS path being the dominant one. Hence, only 2 or 3 multipaths per user are considered in the simulation. Table I shows the system employed for Monte-Carlo simulations.

The parameters follow a uniform distribution in their respective intervals i.e., the DOD and DOA between 0 and 360 degrees, the delays between 0 to $\mathcal{N}_c\mathcal{N}_{sc}T_s - 1$, the Doppler between 0 and 10 kHz and the complex path coefficients follow a uniform phase distribution between 0 and 360 degrees and the gain follows a Rayleigh distribution. Also, for the sake of simplicity, a steering vector towards the dominant multipath is utilised as the transmit weight vector per user.

A. Channel Estimation Studies

In this section, the channel estimator block, illustrated in Fig 4, is evaluated in terms of its performance in the presence of interference and noise. Consider one desired user operating in the presence of 4 co-channel interfering users in a frequency selective channel with 3 paths per user. Let us assume an observation interval of 200 channel symbols ($L = 200$) during which the channel parameters of the desired user to be estimated are $(140\ T_s, 20$ m.s$^{-1}, 60^\circ)$, $(110\ T_s, 66$ m.s$^{-1}, 200^\circ)$ and $(30\ T_s, 120$ m.s$^{-1}, 280^\circ)$. All users are assumed equipowered with an input SNR of 20 dB. Note that SNR is defined as the power of the transmitted signal over the power of the noise. Received signal data generated using random transmitted signal data for the above environment corresponding to $L = 200$ was utilised to obtain the results of the proposed approach as shown in Fig 5.

TABLE I: Simulation Parameters

Parameter	Value	Parameter	Value
F_c	20 GHz	T_s	0.1μs
$\overline{N}$	16	N	9
$\mathcal{N}_c$	15 chips	$\mathcal{N}_{sc}$	5 subcarriers
M	4 users	K	2 paths per user

An important parameter in subspace based approaches is the number of snapshots L used in the estimation procedure. As the value of L increases, the practical covariance matrix provides a better approximation of the theoretical covariance matrix. Figure 6a shows the root mean square error (RMSE) as a function of SNR$\times L$ averaged over 100 trials for all the subspace based approaches in the estimator for a fixed value of L at 200 and equal powers for all users. The SNR was varied from 5 to 30 dB for the simulation. The error in the estimation of the delay is not shown since it is zero through the whole range of SNR$\times L$. The results indicating a decrease in RMSE with increasing values of SNR$\times L$ is in-line with the performance bounds presented in Section II-D. A higher value of L may yield better means to combat lower SNR at the cost of the assumption that the channel remains constant over this longer interval of time. The CRB for the DOA parameter for the proposed spatiotemporal system was presented in Section II-D. Figure 6b presents an evaluation of the proposed algorithm against this theoretical result in terms of the variance of the DOA estimation error. It can be observed that the performance of the proposed system approaches the theoretical bound closely.

B. Reception Studies

Performance and results obtained at the reception stage, illustrated in Fig 4, are presented in this subsection. Due to the

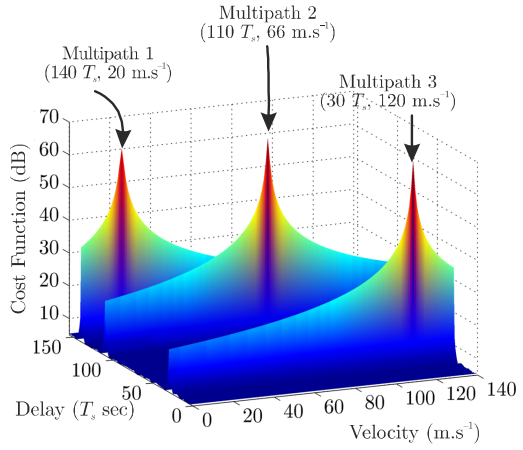

(a) Estimation of the delay-velocity for the three multipaths of the desired user.

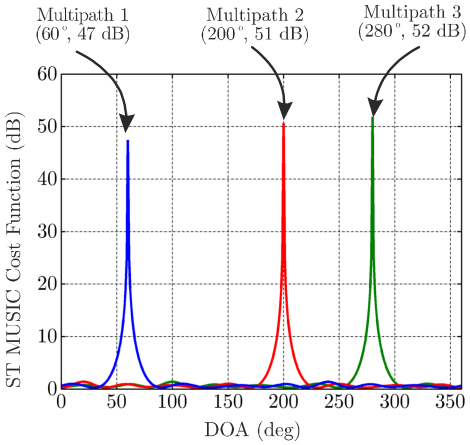

(b) Estimation of the DOA for the three multipaths of the desired user.

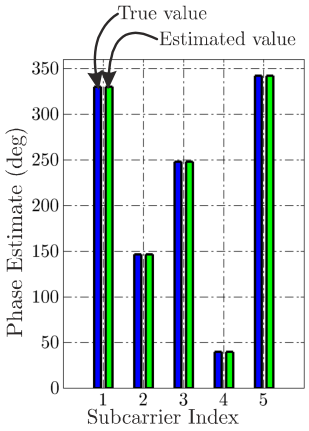

(c) Phase estimate of the elements of the parameter vector $\underline{\gamma}$ for one multipath over all subcarriers.

Fig. 5: Desired user's channel parameter estimation using a circular array of 9 elements operating in the presence of 4 equipowered users with $\mathrm{SNR_{in}} = 20$ dB with $\mathcal{N}_c = 31$ and $\mathcal{N}_{sc} = 5$ (a) Joint delay-velocity estimation (b) DOA estimation (c) Phase estimation of $\underline{\gamma}$.

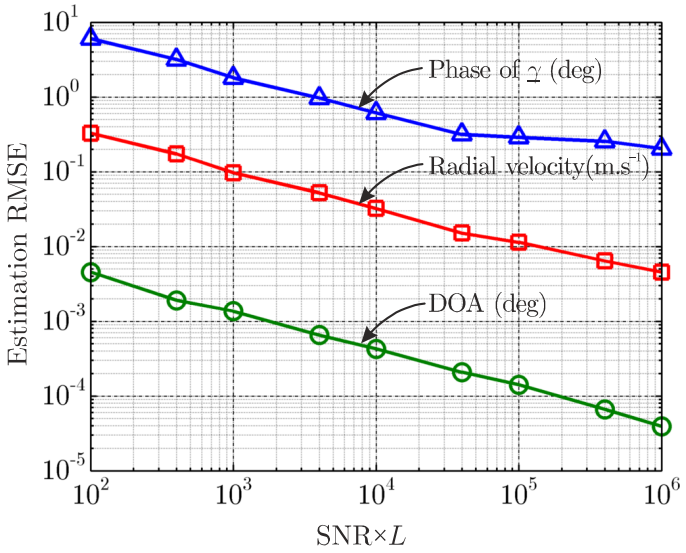

(a) RMSE estimation error of the radial velocity, DOA and phase of $\underline{\gamma}$.

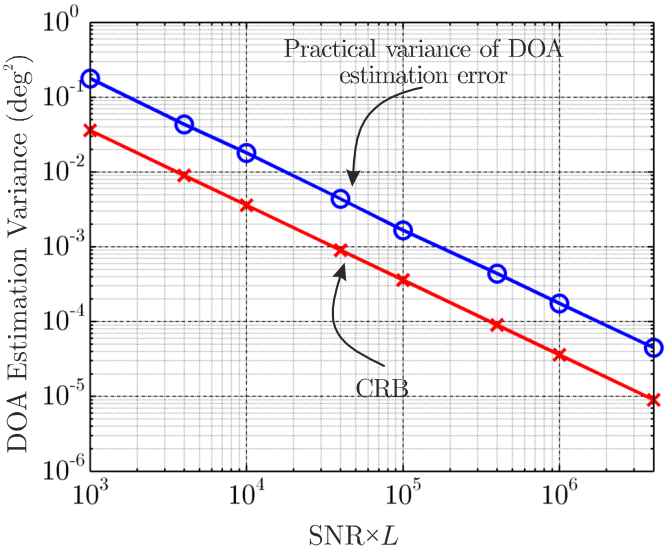

(b) CRB and practical variance of DOA estimation error of the proposed algorithm.

Fig. 6: Evaluation of the proposed spatiotemporal estimator algorithm.

utilisation of the space and time dimensions, the antenna array sets high gains towards the three paths of the desired user and combines them to exploit multipath diversity. For a system operating with the array geometries described in Equs 50 and 51 along with $\mathcal{N}_c = 31$ chips and $\mathcal{N}_{sc} = 5$ subcarriers, Fig 7a illustrates the beampattern[4] of the proposed Doppler-STAR-subspace receiver. It can be observed that the proposed spatiotemporal beamformer provides a maximum gain of 1395 ($N\mathcal{N}_c\mathcal{N}_{sc}$) as compared to a space-only beamformer that would yield a maximum array gain of 9 (N). Figure 7b shows the performance of a massive MIMO beamformer (space-only) consisting of 500 antennas. It is clear from Figs. 7a and 7b that, although the spatiotemporal beamformer utilises a smaller number of antennas (only 9) than the massive MIMO beamformer, it achieves a much higher gain making it suitable to address the issues of high path loss in 5G mm-wave communications. Note also that the spatiotemporal approach can be used with any array geometry containing any number of sensors. Thus, if it is employed in conjunction with a massive Rx antenna array of 500 antennas, the gains would be massive as this is shown in Fig 8.

Consider again the simulation environment of Fig 7, but this time let us assume that two out of the three paths of the desired user are co-directional (DOA = 280°). Consider also that the DOA of one of the "unwanted" is 280°. Figure 9 shows the array gain pattern of the proposed beamformer of

[4]Here, for the sake of the simplicity, the Doppler frequency of the multipaths of the first user are equal.

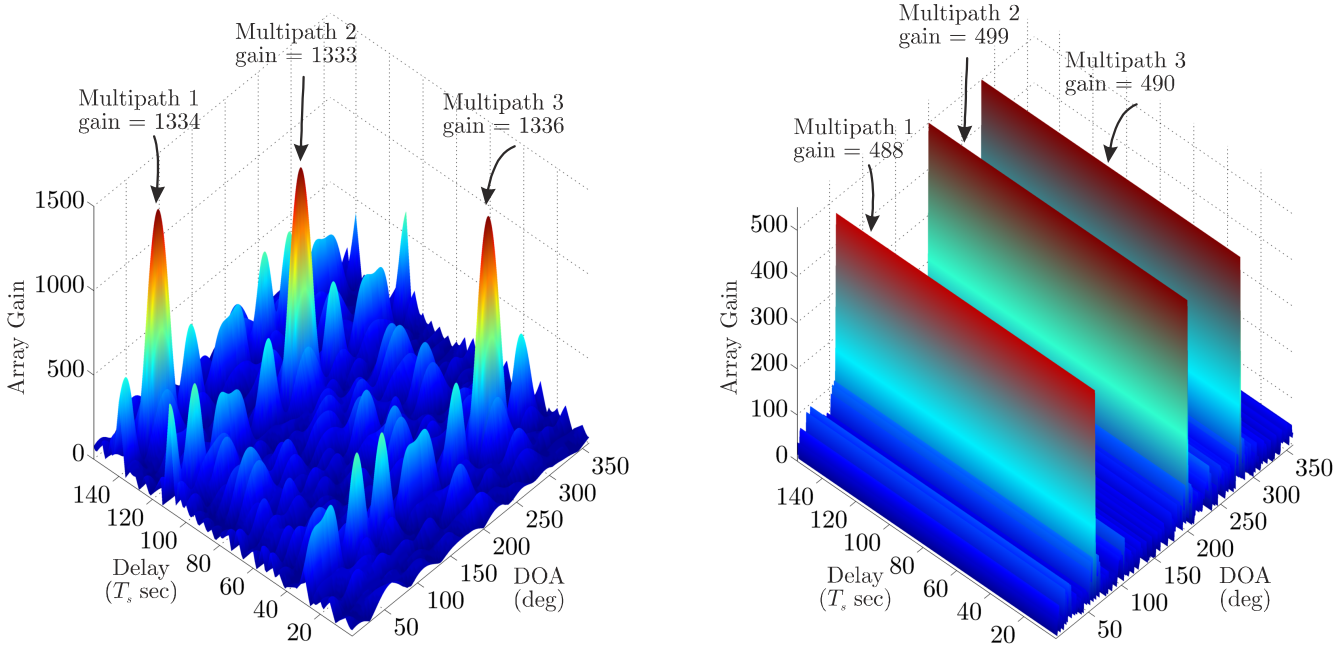

(a) Beampattern of a Doppler-STAR-subspace receiver consisting of 9 antenna elements

(b) Beampattern of a massive MIMO subspace receiver consisting of 500 antenna elements

Fig. 7: Comparison of the beampatterns of the proposed Doppler-STAR approach and a spatial-only massive MIMO system.

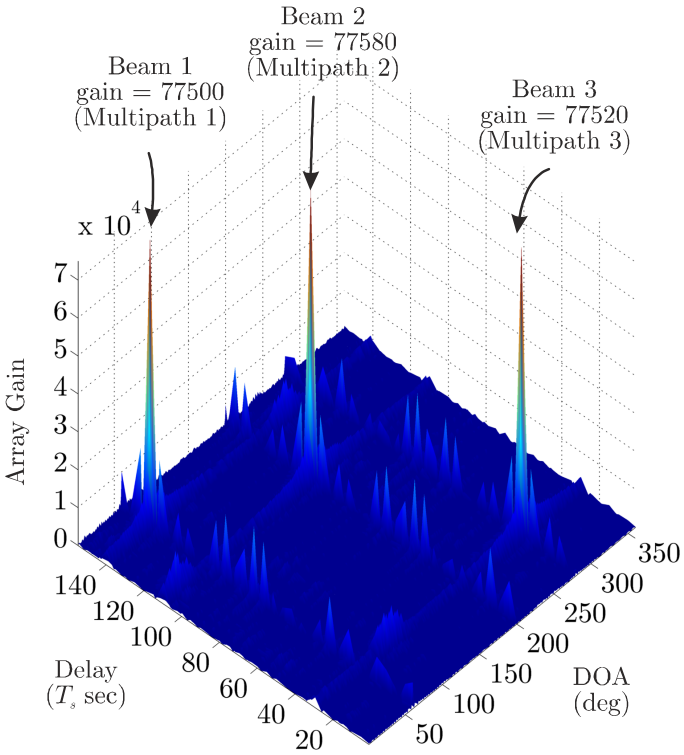

Fig. 8: Beampattern of a spatiotemporal massive MIMO system with 500 antennas.

9 antennas and a traditional massive MIMO of 500 antennas. Figure 9a shows that the proposed Doppler-STAR-subspace receiver has 3 mainlobes with very high gains even for the two co-directional paths (2nd and 3rd) and suppresses the co-directional interference too. However, Fig 9b shows that a traditional massive MIMO beamformer cannot distinguish the 2nd and 3rd paths of the desired user (hence cannot exploit the multipath diversity) while also receives the 280° signal of the "unwanted" user with very high gain.

Figure 10 shows the performance of the proposed Doppler-STAR-subspace receiver (whose weights are given by Equ 44) against other spatiotemporal receivers such as the Doppler-STAR-RAKE (Equ 47), Doppler-STAR-decorrelating (Equ 49) and traditional spatial-only massive MIMO (500 antennas) beamformer (enhanced with subspace set of weights and RAKE weights) in the presence of high interference and noise in terms of the output SNIR (SNIR_{out}). Note that, in these comparative studies, identical transmitter structures and transmitted data (from point-A to point-F in Fig 2) are utilised for all receivers, generating signals of the same bandwidth. The $\text{SNIR}_{j,\text{out}}$ parameter is the level of interference in the beamformed signal of the j-th subcarrier and evaluates the performance of the reception system to mitigate interferences. The estimation of this parameter is based on $\mathbb{R}_{\text{ISI}}+\mathbb{R}_{\text{MAI}}+\mathbb{R}_{\text{nn}}$, the covariance matrix of the undesired components of the received signal, and $\mathbb{R}_{\text{des}}$, the covariance matrix of the desired signal

$$\text{SNIR}_{j,\text{out}} = \frac{\underline{w}_j^H \mathbb{R}_{\text{des}} \underline{w}_j}{\underline{w}_j^H \left(\mathbb{R}_{\text{ISI}} + \mathbb{R}_{\text{MAI}} + \mathbb{R}_{\text{nn}}\right) \underline{w}_j}. \tag{52}$$

By employing a Doppler-STAR-RAKE receiver that does not perform interference cancellation, the expression simplifies to

$$\text{SNIR}_{j,\text{out}} = N\mathcal{N}_c\mathcal{N}_{sc}\frac{P_s}{\sigma_{\text{n}}^2 + P_{\text{int}}}, \tag{53}$$

where P_{int} is the residual power contribution from MAI and ISI. By appropriately designing the Doppler-STAR-subspace

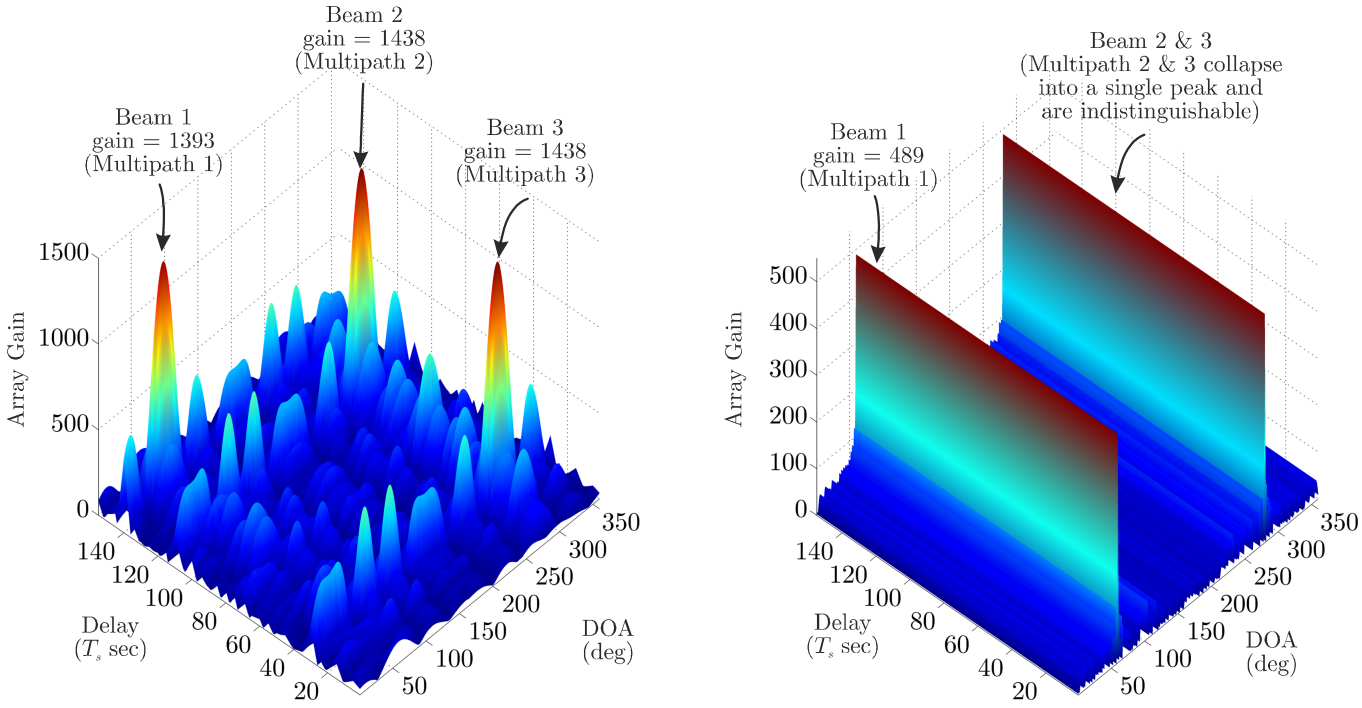

(a) Beampattern of a Doppler-STAR-subspace receiver consisting of 9 antenna elements

(b) Beampattern of a massive MIMO subspace receiver consisting of 500 antenna elements

Fig. 9: Comparison of the beampatterns of the proposed Doppler-STAR approach and a spatial-only massive MIMO system in a scenario where two multipaths arrive with the same DOA albeit different path delays

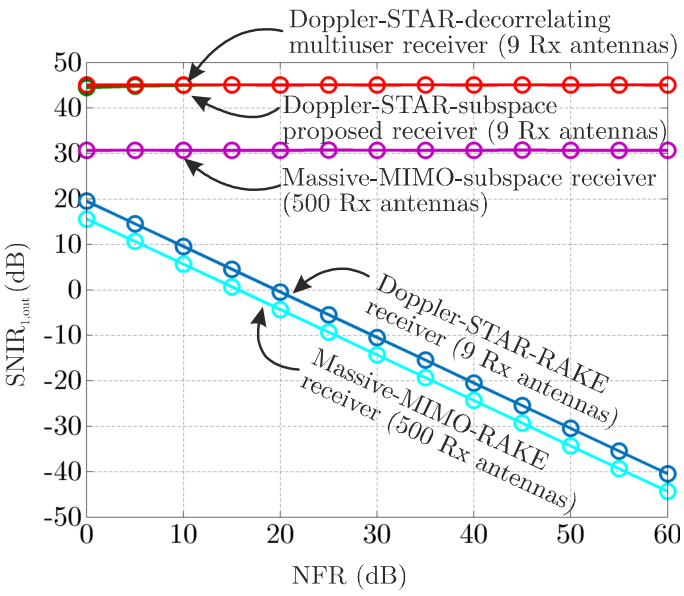

Fig. 10: Comparative study of the performance of the proposed Doppler-STAR subspace receiver with other spatiotemporal and spatial-only receivers in terms of the NFR. (200 trials).

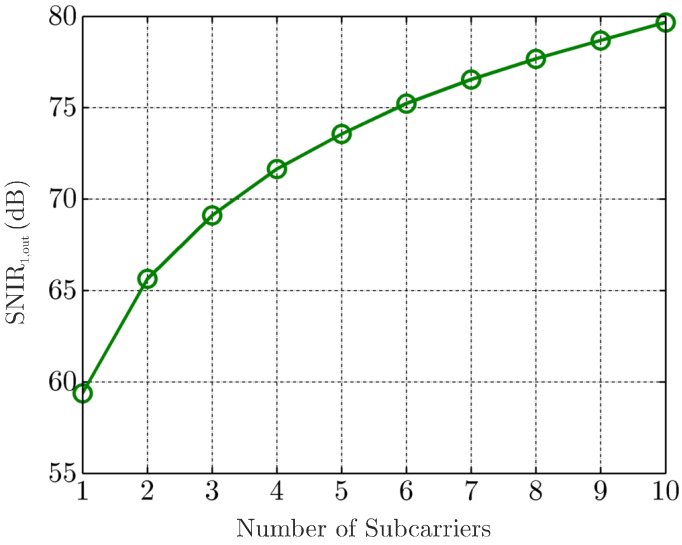

Fig. 11: Performance of the Doppler-STAR-subspace receiver with increasing number of subcarriers with data copy over subcarriers (50 trials).

weights, this expression simplifies to

$$\text{SNIR}_{j,\text{out}} = N\mathcal{N}_c\mathcal{N}_{sc}\text{SNR}_{\text{in}}, \tag{54}$$

there is complete interference cancellation ($P_{\text{int}} \to 0$). As expected, the SNIR$_{1,\text{out}}$ of the Doppler-STAR-RAKE receiver decreases dramatically. This illustrates that the Doppler-STAR-RAKE receiver is unable to provide appropriate levels of performance in the presence of interference. On the other hand, the Doppler-STAR-subspace receiver, provides steady performance over a huge range of NFR from 0 to 60 dB

by incorporating terms to explicitly suppress interference. Tolerance to the near-far problem is critical in cells with high user density. Also, the proposed Doppler-STAR-subspace receiver of 9 antennas outperforms the traditional massive MIMO beamformer of 500 antennas by 15 dB. Note that in the traditional massive MIMO beamformer, "subspace" and "RAKE" weights have been utilised which are in fact superior to the conventional massive MIMO beamformers such as "steering vector", "Weiner-Hopf" or "Capon" beamformers. As illustrated in Fig 10, a performance very close to a multi user receiver (Doppler-STAR-decorrelating receiver) is obtained without the channel knowledge of the interferers. The performance is also an indicator that at varying NFR levels, the channel estimation errors, if any, lie within the input error tolerance boundary of the receiver.

Figure 11 presents the performance of the proposed receiver with increasing number of subcarriers. Simulations show that the Doppler-STAR-subspace receiver exploits the frequency diversity to provide a higher SNIR_{out}. Also, degrees of freedom may be added by using a spatiotemporal approach at the transmitter side too. In this paper, we do not exploit the overall Tx-Rx geometry by employing the concept of virtual MIMO. This may be a further extension of the current work.

V. Conclusion

In this paper, a novel parametric channel model for mm-wave environments has been proposed. Based on this model, a spatiotemporal beamformer performing channel estimation and reception has been designed. This beamformer was evaluated with varying levels of noise and interference. Simulation results indicate that the estimation and reception processes are highly tolerant to the near-far problem and yield a performance 15dB better than the traditional MIMO system of 500 antennas, exhibiting very high array gain and selectivity in space and time. This would enable the system to function without power control management algorithms. It is important to point out that the proposed receiver belongs to the family of spatiotemporal (space-time) receivers that exploits the spatiotemporal degrees of freedom and employs a beamformer that automatically combines multipath and suppresses co-channel interferences from other users to obtain an array gain similar to that of a massive MIMO system with a much smaller number of antennas. Finally, although the proposed approach is designed for the mm-wave frequency band, it is applicable to any radio frequency band. These characteristics of the presented system make it an attractive option for the next generation of mobile systems.

Appendix

Simplification to Single-Carrier System: In the case of a single-carrier simplification of the proposed spatiotemporal multicarrier system, $\mathcal{N}_{sc}$ becomes equal to one and therefore, the subscript j, corresponding to the j-th subcarrier, may now be dropped in all the expressions and in Fig 2. Thus, in this case, Fig 2 simplifies to Fig 12.

References

[1] G. R. Maccartney Jr, J. Zhang, S. Nie, and T. S. Rappaport, "Path loss models for 5G millimeter wave propagation channels in urban microcells," in *IEEE Global Conference on Communications*, Dec. 2013, pp. 3948–3953.

[2] H. Yang, P. Smulders, and M. Herben, "Channel characteristics and transmission performance for various channel configurations at 60 GHz," *EURASIP Journal on Wireless Communications and Networking*, vol. 2007, no. 1, May 2007.

[3] S. Akoum, O. El Ayach, and R. W. Heath, "Coverage and capacity in mmWave cellular systems," in *IEEE ASILOMAR Conference on Signals, Systems and Computers*, Nov. 2012, pp. 688–692.

[4] E. Torkildson, H. Zhang, and U. Madhow, "Channel modeling for millimeter wave MIMO," in *IEEE Workshop on Information Theory and Applications*, Jan. 2010, pp. 1–8.

[5] W. Roh, J. Y. Seol, J. Park, B. Lee, J. Lee, Y. Kim, J. Cho, K. Cheun, and F. Aryanfar, "Millimeter-wave beamforming as an enabling technology for 5G cellular communications: Theoretical feasibility and prototype results," *IEEE Communications Magazine*, vol. 52, pp. 106–113, Feb. 2014.

[6] B. Yin, S. Abu-surra, G. Xu, T. Henige, E. Pisek, Z. Pi, and J. R. Cavallaro, "High-throughput beamforming receiver for millimeter wave mobile communication," in *IEEE Global Conference on Communications*, Dec. 2013, pp. 3802–3807.

[7] G. H. Song, J. Brady, and A. Sayeed, "Beamspace MIMO transceivers for low-complexity and near-optimal communication at mm-wave frequencies," in *IEEE International Conference on Acoustics, Speech and Signal Processing*, May 2013, pp. 4394–4398.

[8] T. S. Rappaport and S. Sun, "Multi-beam antenna combining for 28 GHz cellular link improvement in urban environments," in *IEEE Global Conference on Communications*, Dec. 2013, pp. 3859–3864.

[9] Jinho Choi, "On coding and beamforming for large antenna arrays in mm-Wave systems," *IEEE Wireless Communications Letters*, vol. 3, no. 2, pp. 193–196, Apr. 2014.

[10] O. E. Ayach, S. Rajagopal, S. Abu-Surra, Z. Pi, and R. W. Heath, "Spatially sparse precoding in millimeter wave MIMO systems," *IEEE Transactions on Wireless Communications*, vol. 13, no. 3, pp. 1499–1513, Mar. 2014.

[11] A. Alkhateeb, O. E. Ayach, G. Leus, and R. W. Heath, "Channel estimation and hybrid precoding for millimeter wave cellular systems," *IEEE Journal of Selected Topics in Signal Processing*, vol. 8, no. 5, pp. 831–846, Oct. 2014.

[12] X. Huang, Y. J. Guo, and J. D. Bunton, "A hybrid adaptive antenna array," *IEEE Transactions on Wireless Communications*, vol. 9, no. 5, pp. 1770–1779, May 2010.

[13] J. Nsenga, A. Bourdoux, and F. Horlin, "Mixed analog/digital beamforming for 60 GHz MIMO frequency selective channels," in *IEEE International Conference on Communications*, May 2010, pp. 1–6.

[14] M. Choi, G. Grosskopf, D. Rohde, B. Kuhlow, G. Przyrembel, and H. Ehlers, "Experiments on DOA-estimation and beamforming for 60 GHz smart antennas," in *IEEE Semiannual Vehicular Technology Conference*, vol. 2, Apr. 2003, pp. 1041–1045.

[15] S. Affes, H. Hansen, and P. Mermelstein, "Interference subspace rejection: a framework for multiuser detection in wideband CDMA," *IEEE Journal on Selected Areas in Communications*, vol. 20, no. 2, pp. 287–302, Feb. 2002.

[16] Y. Zhang and M. Amin, "Array processing for nonstationary interference suppression in DS/SS communications using subspace projection techniques," *IEEE Transactions on Signal Processing*, vol. 49, no. 12, pp. 3005–3014, Dec. 2001.

[17] A. Manikas, *Differential Geometry in Array Processing*. Imperial College Press, 2004.

[18] G. Efstathopoulos and A. Manikas, "Extended array manifolds: Functions of array manifolds," *IEEE Transactions on Signal Processing*, vol. 59, no. 7, pp. 3272–3287, Jul. 2011.

[19] P. D. Karaminas and A. Manikas, "Super-resolution broad null beamforming for cochannel interference cancellation in mobile radio networks," *IEEE Trans. Vehicular Technology*, vol. 49, no. 3, pp. 689–697, may 2000.

[20] A. Manikas and M. Sethi, "A space-time channel estimator and single-user receiver for code-reuse DS-CDMA systems," *IEEE Transactions on Signal Processing*, vol. 51, no. 1, pp. 39–51, Jan. 2003.

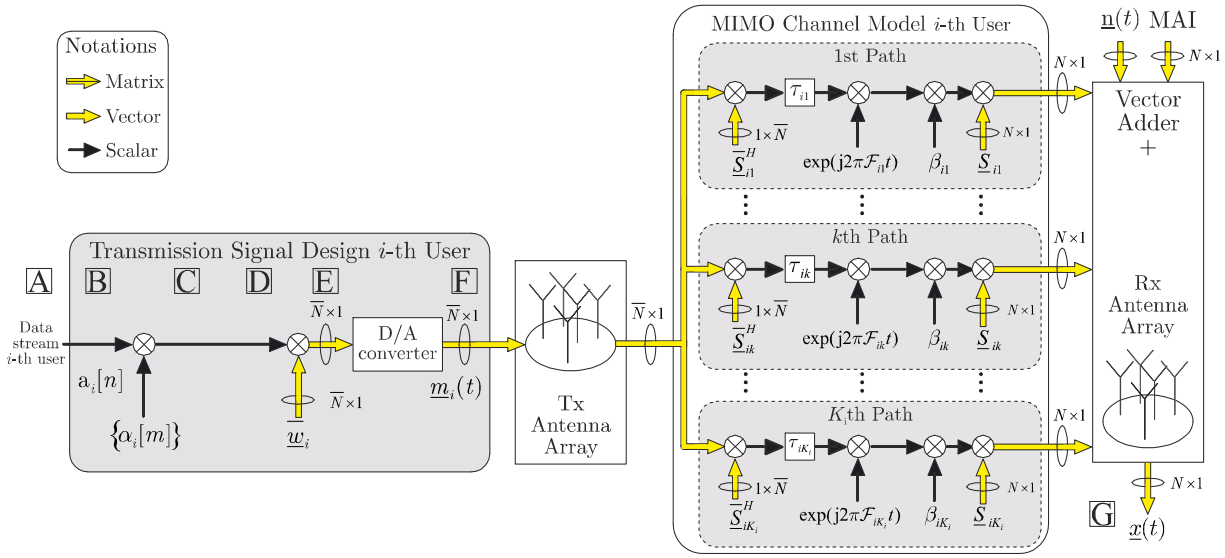

Fig. 12: Baseband representation of the transmitter and the MIMO channel for the i-th user of the SC-DS-CDMA system.

Vidhya Sridhar received the B.Tech. degree in electronics and communication engineering from National Institute of Technology, Trichy, India in 2009. She received the M.Sc. degree in communications and signal processing from Imperial College London, London, U.K. in 2012. She graduated with distinction and was awarded the Outstanding Achievement Prize as the top of the class M.Sc. student.

From 2009 to 2011, she was with CDOT Alcatel Lucent Research Centre, Chennai, India. From 2012 to 2013, she was with Broadcom Pvt. Ltd, Bangalore, India. Since 2013, she has been pursuing the Ph.D. degree under the supervision of Prof. A. Manikas in the Communications and Signal Processing Group.

She has been awarded the Imperial College Ph.D. Scholarship to pursue her research. Her research interests include flexible array signal processing, 5G, array communications, source localisation and tracking.

Thibaud Gabillard received the Dipl.Ing. degree in signal processing and communications from École Supérieure d'Électronique de l'Ouest, Angers, France in 2013. He received the M.Sc. degree in signal processing from Université de Rennes I, Rennes, France in 2013.

In 2013, he was with Thales Communications & Security, Cholet, France. In 2012, he was with the British Geological Survey, Edinburgh, U.K.. Since 2013, he has been pursuing the Ph.D. degree under the supervision of Prof. A. Manikas in the Communications and Signal Processing Group, Department of Electrical and Electronic Engineering, Imperial College London, London, U.K..

Thibaud Gabillard was part of the organizing committee of IEEE International Conference on Communications (ICC) 2014. His research is fully funded by the Engineering and Physical Science Research Council Doctoral Training Award. His research interests are arrayed wireless communication systems, interference cancellation and differential geometry.

Professor A. Manikas has been with the Department of Electrical and Electronic Engineering at Imperial College London since 1988, where he holds the Chair of Communications and Array Signal Processing.

He has held a number of research consultancies for the EU, industry and government organisations. He is on various Editorial Boards and has had various technical chairs at international conferences including the TPC Chair of IEEE ICC 2015 in London. He has published an extensive set of journal and conference papers in the areas of wireless communications and array signal processing and is the author of a monograph entitled "Differential Geometry in Array Processing". His main research interests include: space-time wireless communications, antenna arrays, array signal processing, beamforming, localization, uncertainties, mathematical modelling, analysis and algorithmic design, radar signal processing, MIMO radar, wireless sensor networks, 5G+, physical layer. He is leading a strong group of researchers at Imperial College and has supervised successfully more than 45 PhDs and more than 200 Masters project-students.

Professor Manikas is a Fellow of the Institution of Engineering and Technology (IET), Fellow of the Institute of Mathematics and its Applications (IMA) and a Distinguished Lecturer of IEEE Communications Society. He is also the vice-Chair of IEEE COMSOC TAOS Technical Committee.